Exponential Asymptotics for Dark Solitons of the Discrete NLS Model

C. J. Lustri,[1] P. G. Kevrekidis,[2,3,4] and D.E. Pelinovsky[5]

[1]*School of Mathematics and Statistics, The University of Sydney, Camperdown 2050, Australia*
[2]*Department of Mathematics and Statistics, University of Massachusetts Amherst, Amherst, MA 01003, USA*
[3]*Department of Physics, University of Massachusetts Amherst, Amherst, MA 01003, USA*
[4]*Department of Mechanical Engineering, Seoul National University, 1 Gwanak-ro, Gwanak-gu, Seoul 08826, South Korea*
[5]*Department of Mathematics, McMaster University, Hamilton, Ontario, Canada*

In the present work we revisit the problem of the dark solitary wave pinned in the discrete nonlinear Schrödinger equation. In a number of recent studies, the methodology of exponential asymptotics was attempted to be utilized in this problem, however the results were not found to be fully in agreement with associated multiprecision numerical computations. Here we resolve this conundrum by finding precise exponential asymptotics for the pinned dark solitary waves. Moreover, we reconcile the relevant result with a general theory of pinned dark solitary waves in the *continuum* nonlinear Schrödinger equations in the presence of external potentials.

I. INTRODUCTION

The study of discrete nonlinear dispersive systems and of the effects of the underlying lattice on the dynamics of solitary waves has a long history of over half a century [36] that has by now been summarized in numerous reviews [7, 8], as well as books [17, 33]. The relevant features concern the existence of the famous Peierls-Nabarro barrier [22], its dynamical implications on the mobility of kinks [36] and discrete solitary waves [10, 31], the existence of discrete breathers [8, 26] (and their mobility [9]), as well as the existence of discrete vortices [6, 13, 28], among many others.

A key feature of discreteness is that it breaks continuous symmetries, such as most notably translational invariance, but also potentially others such as the so-called conformal (scaling) invariance of the 2d nonlinear Schrödinger (NLS) model [18]. This paves the way for approaching the continuum limit in different ways. For instance, even within the same continuum model, such as, e.g., the NLS or sine-Gordon, and for a single discretization of such a model respectively —e.g., the discrete NLS (DNLS) [17] or the discrete sG [36]— there exist multiple stationary discrete solitary waves that correspond to the same continuum solitary wave. I.e., there is an onsite (site-centered) and an intersite (intersite-centered) version of a solitary wave, one of which turns out to be spectrally stable and the other one turns out to be spectrally unstable, both of which approach the same continuum solitary wave limit as the spacing distance between lattice nodes tends to 0. However, additionally [17, 18], even for the same continuum model, there may exist *multiple discretizations* (in the same way in which we envision multiple discretizations in numerical analysis) which may preserve (or "destroy") different symmetries. A characteristic example at the NLS level is —in addition to the standard DNLS discretization— the famous integrable Ablowitz–Ladik discretization [1]. The latter preserves infinitely many conservation laws and has, accordingly, continuous families of solitary waves compared to the onsite and intersite states in the DNLS model.

In the present work we revisit one of the quintessential features that discreteness *generically* introduces in nonlinear dynamical systems, namely the implications of translation invariance breaking to the eigenvalues of the spectral stability problem for the discrete solitary waves as the continuum limit is approached. This is a topic that has been explored extensively in the DNLS model for at least a quarter of a century, both at the level of bright solitary waves (of the focusing DNLS) [12], as well as for dark solitary waves (of the defocusing DNLS) [14]. It is important to appreciate here that part of the interest in the subject stems from the fact that this is not a feature particular to this model but the breaking of translational invariance will *very broadly* bear such implications in discrete models, unless the models are constructed in a way such that they preserve translational invariance [32]. It was recognized already quite early (and was accordingly quantified [15]) that the breaking of translational invariance should be beyond all

algebraic orders in the expansion of a discrete difference operator in continuum derivatives. Indeed, such early works as [15] were able to capture the exponentially small behavior of associated eigenvalues to the continuum limit (as well as the corresponding power law "modulating" this exponential dependence). However, for technical reasons related to the methods used, such approaches were unable to identify the relevant prefactor (or for that matter the correction to the leading order exponential asymptotics).

Remarkably, recent efforts have brought to bear advanced *exponential asymptotics* techniques to bridge this gap and provide definitive closure to the dependence of the relevant eigenvalues both as regards the exponential and power-law dependences of the prefactor on the lattice spacing, but also of the numerical prefactor [2, 25], as well as of the leading order correction [25]. Indeed, relevant techniques were extended to other problems, such as, e.g., ones involving next-nearest-neighbors [24]. Importantly, also, concurrent developments in numerical computation have enabled the identification of relevant eigenvalues with unprecedented accuracy, enabling their monitoring over *many* decades of data, which, in turn, has allowed to test the accuracy of both the leading order predictions, but also that of the associated next-order corrections [23].

Interestingly, the above developments can now be considered to be *definite* (as described in the above paragraph) *solely* for the case of bright solitons of the focusing NLS model that asymptote to a vanishing background. The realm of dark solitons of the defocusing DNLS model —asymptoting to two opposite non-vanishing constants— has proven to be far more elusive. Here, comparison of theoretical attempts and numerical findings has been *unsuccessful* [2] and even the most recent numerical efforts [23] have at best only provided numerical fits to the eigenvalue data. The dark soliton case, as was already shown in the seminal work of [14] is far more technically involved as the continuous spectrum of these solitary waves encompasses the entire imaginary axis as the continuum limit is approached. Among the two cases of the onsite and intersite discrete solitary waves, the one that is easier to numerically monitor is the intersite one, involving always a real eigenvalue pair, immediately upon departure from the well-known anti-continuum limit [26, 35] of uncoupled sites to the continuum limit of vanishing spacing (and effectively infinite coupling) between them. Even for that case, and despite the most recent highest accuracy numerics [23], no theory has captured the numerical prefactor (or the next-order-correction) to this date, to the best of our knowledge. Far more subtle is the case of the onsite mode where the translational eigenvalue starts on the imaginary axis in the anti-continuum limit [35] and upon a collision with the continuous spectrum that was definitively displayed in [14], becomes a *quartet* of eigenvalues in the complex plane. The relevant complex eigenvalue is exceptionally difficult to technically capture as has been illustrated not only in the seminal efforts of [14], but even within the most recent study of [23] (which has aimed to fit this eigenvalue only up to $h \approx 0.9$).

The aim of the present work is to *definitively* address this issue through the use of delicate exponential asymptotics that account effectively also for the role of the continuous spectrum. Our efforts are significantly inspired from the work of [34], which, in addition to a Melnikov analysis for the persistence conditions of dark solitons in the perturbed continuum NLS equation, had developed a stability analysis of the pinned dark solitary waves that also had the same pathological characteristic of the splitting of small eigenvalues due to an external potential breaking translational invariance and due to the continuous spectrum which admits no spectral gap near the origin. In that case too, the eigenvalues when not directly real would move into the complex plane, as we find here too. Indeed, we are able to identify both the leading order prefactor of the real eigenvalues for the intersite discrete soliton case, and the corresponding correction term. Similarly, in the onsite case, we are able to trace the complex eigenvalues and we come as close as we have found it to be numerically possible to identifying the associated real and imaginary parts. In addition to the state-of-the-art analytical findings, multiprecision numerical techniques have been used to obtain many decades of numerical eigenvalues, allowing the definitive testing of our findings.

Our presentation is structured as follows. Section II presents the model setup and the existence analysis for the discrete dark solitary waves with the account of the exponential small terms. Section III lies at the center of our exposition and presents our stability results. Section IV corroborates our findings through detailed numerical computations of both intersite and onsite eigenvalue configurations. Finally, section V summarizes our findings and presents our conclusions.

II. MATHEMATICAL SETUP AND EXISTENCE THEORY

Starting with the standard DNLS model [17]

$$i\dot{u}_n = -C(u_{n+1} + u_{n-1} - 2u_n) + |u_n|^2 u_n, \tag{1}$$

we consider, as is common within this model, the case of standing waves of the form (setting the background amplitude/frequency to unity without loss of generality) $u_n = e^{-it}\phi_n$. Also, in order to connect with the continuum limit we use $C = 1/h^2$, aiming to characterize the limit of $h \to 0$, rather than the anti-continuum limit of $C \to 0$.

The governing steady state model accordingly reads:

$$\frac{1}{h^2}(\phi_{n+1} - 2\phi_n + \phi_{n-1}) - (|\phi_n|^2 - 1)\phi_n = 0. \tag{2}$$

Let $z = hn$ and $\tilde{z} = z - z_0$ with $z_0 \in \mathbb{R}$ to be defined. Expanding Eq. (2) in powers of h^2 gives

$$2\sum_{m=1}^{\infty} \frac{h^{2m-2}}{(2m)!} \frac{\mathrm{d}^{2j}\phi(\tilde{z})}{\mathrm{d}\tilde{z}^{2j}} + (\phi(\tilde{z})^2 - 1)\phi(\tilde{z}) = 0, \tag{3}$$

where we have made the assumption that $\phi(\tilde{z})$ is real-valued for real $\tilde{z}$. We are looking for the power series solution of Eq. (3) given by

$$\phi(\tilde{z}) \sim \sum_{j=0}^{\infty} h^{2j}\phi_j(\tilde{z}) \quad \text{as} \quad h \to 0, \tag{4}$$

where we have abused notation slightly by using subscripts to indicate the series index, as opposed to the value of the lattice index n, for the sake of later notational convenience. We select the leading-order solution that tends to the dark solitary wave in the continuum limit,

$$\phi_0(\tilde{z}) = \tanh\left(\frac{\tilde{z}}{\sqrt{2}}\right). \tag{5}$$

This leading-order solution is singular at $\tilde{z}_s = \mathrm{i}\pi/\sqrt{2} + k\sqrt{2}\pi\mathrm{i}$ for $k \in \mathbb{Z}$. The important singularities are $k = 0$ and -1, which are located at complex conjugate positions. The recurrence relation for the series terms is Expanding this gives

$$2\sum_{m=1}^{j} \frac{1}{(2m)!} \frac{\mathrm{d}^{2j}\phi_{j-m+1}}{\mathrm{d}\tilde{z}^{2j}} + (3\phi_0^2 - 1)\phi_j = 0. \tag{6}$$

We can use the recurrence relation to obtain the particular solution for $\phi_1(\tilde{z})$, given by

$$\phi_1(\tilde{z}) = -\frac{1}{48}\operatorname{sech}^2\left(\frac{\tilde{z}}{\sqrt{2}}\right)\left(9 + 2\sqrt{2}\tilde{z} - 8\tanh\left(\frac{\tilde{z}}{\sqrt{2}}\right)\right). \tag{7}$$

This will allow us to find the first correction in h to the eigenvalue calculation. The late-order behaviour has the form

$$\phi_j(\tilde{z}) \sim \frac{\Phi(\tilde{z})\Gamma(2j+\gamma)}{\chi(\tilde{z})^{2j+\gamma}} \quad \text{as} \quad n \to \infty, \tag{8}$$

where $\chi(\tilde{z}) = 0$ at $\tilde{z} = \tilde{z}_s$. Using the same techniques as [25], we find that the singulant is given by

$$\chi(\tilde{z}) = 2\pi\mathrm{i}\ell(\tilde{z} - \tilde{z}_s), \qquad \ell \in \mathbb{Z}, \tag{9}$$

where we are concentrating on $\ell = \pm 1$. This means that the Stokes lines emerge from the singularity at $\tilde{z} = \tilde{z}_s$ and follow the imaginary axis, as in [25]. This is shown in Figure 1. The prefactor equation becomes

$$\Phi'' - (3\phi_0^2 - 1)\Phi = 0, \tag{10}$$

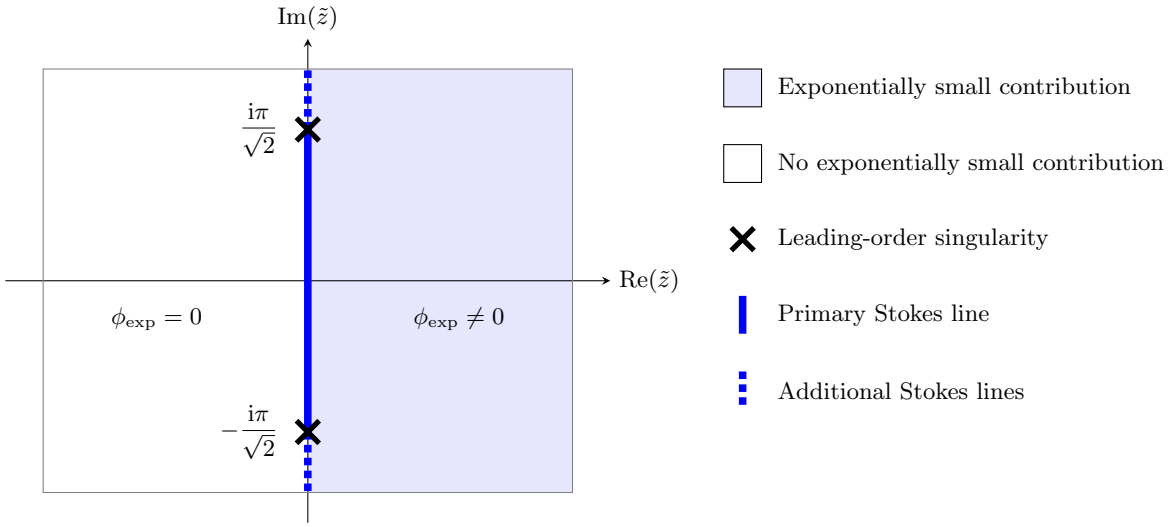

Figure 1: Stokes structure for the discrete solitary wave solution. The relevant Stokes line is shown as a solid blue line. There are additional singularities further along the imaginary axis in both directions, but the corresponding Stokes lines switch on asymptotic contributions that are exponentially small compared to those considered here.

so $\Phi(\tilde{z}) = K_1\Phi_1(\tilde{z}) + K_2\Phi_2(\tilde{z})$, where K_1 and K_2 are arbitrary constants, while

$$\Phi_1(\tilde{z}) = \frac{1}{4}\,\text{sech}^2\left(\frac{\tilde{z}}{\sqrt{2}}\right), \tag{11}$$

$$\Phi_2(\tilde{z}) = \frac{1}{2}\Big(6\sqrt{2}\,\tilde{z} + 8\sinh\Big(\sqrt{2}\tilde{z}\Big) + \sinh\Big(2\sqrt{2}\tilde{z}\Big)\Big)\,\text{sech}^2\left(\frac{\tilde{z}}{\sqrt{2}}\right). \tag{12}$$

This choice of homogeneous solution is so that $\Phi_1 \sim \mathrm{e}^{-\sqrt{2}\tilde{z}}$ as $\tilde{z} \to \pm\infty$ and $\Phi_2 \sim \pm\mathrm{e}^{\sqrt{2}\tilde{z}}$ as $\tilde{z} \to \pm\infty$. The parameters γ and K_1 must be determined by considering the late-order terms (8) in the vicinity of $\tilde{z} = \tilde{z}_s$. By using an essentially identical argument to [25], it follows that $\gamma = 4$ and that $K_1 \approx -5\mathrm{i}\Lambda/(4\sqrt{2})$ where $\Lambda \approx 358.464$.

Using a largely unchanged exponential asymptotic analysis in comparison to [25], which was based on the method introduced in [5, 20, 30], it can therefore be shown that the exponentially-small quantity which appears as the Stokes line, shown in Figure 1, is crossed from left to right is given by

$$\phi_{\text{exp}}(\tilde{z}) \sim -\frac{2\pi\mathrm{i}\Phi(\tilde{z})}{h^\gamma}\,e^{-\frac{\chi(\tilde{z})}{h}} + \text{c. c.} \quad \text{as} \quad h \to 0, \tag{13}$$

where c. c. refers to the complex conjugate of this expression. In the limit as $\tilde{z} \to \infty$, this is

$$\phi_{\text{exp}}(\tilde{z}) \sim -\frac{2\pi}{h^4}\left(\frac{5\Lambda}{4\sqrt{2}}\mathrm{e}^{\sqrt{2}\tilde{z}}\right)e^{-\frac{\sqrt{2}\pi^2}{h}}\sin\left(\frac{2\pi\tilde{z}}{h}\right) \quad \text{as} \quad h \to 0,\ \tilde{z} \to \infty. \tag{14}$$

The exponential grows in the limit that $\tilde{z} \to \infty$, which is inconsistent with the requirement that the solution remain bounded on the original discrete sites ($\epsilon z/h \in \mathbb{Z}$) in this limit.

As in the DLNS bright breather case, we can take advantage of the fact that we are free to select z_0 in order to identify solutions in which $\phi_{\text{exp}} = 0$ on discrete sites. By selecting z_0 such that $z_0/h = N$ where $N \in \mathbb{Z}$, we find that

$$\sin\left(\frac{2\pi\tilde{z}}{h}\right) = \sin\left(\frac{2\pi z}{h} - \frac{2\pi z_0}{h}\right) = \sin\left(\frac{2\pi z}{h} - 2\pi N\right) = \sin\left(\frac{2\pi z}{h}\right), \tag{15}$$

which equals 0 if $z/h \in \mathbb{Z}$. This corresponds to site-centered solutions. If we instead select z_0 such that $z_0/h = N + 1/2$ where $N \in \mathbb{Z}$, we obtain

$$\sin\left(\frac{2\pi\tilde{z}}{h}\right) = \sin\left(\frac{2\pi z}{h} - \frac{2\pi z_0}{h}\right) = \sin\left(\frac{2\pi z}{h} - (2N+1)\pi\right) = \sin\left(\frac{2\pi z}{h}\right), \tag{16}$$

which also equals 0 if $z/h \in \mathbb{Z}$. This corresponds to selecting intersite-centered solutions. For both of these configurations, $\phi_{\exp}(\tilde{z}) \to 0$ as $\tilde{z} \to \infty$ on the discrete sites, even though the continuous function $\phi_{\exp}(\tilde{z})$ demonstrates exponentially growing oscillations for other values of $\tilde{z}$ in this limit.

III. STABILITY ANALYSIS

Obtaining the leading-order approximation to the eigenvalues as in [25] indicates that the intersite-centered solutions should be unstable with a pair of real eigenvalues near the origin while the site-centered solutions are stable with a pair of purely imaginary eigenvalues near the origin. However, we know from [34] that, in the latter cae, the pair of eigenvalues splits off the purely imaginary axis as a complex quadruplet. To explain this splitting, we must find the first correction in the expansions for the small eigenvalues in small h. This analysis is proximal to that of [34] in some respects; however, there are key differences that are presented.

We introduce the usual perturbation $\phi = \phi_s + fe^{\lambda t} + g^* e^{\lambda^* t}$, where ϕ_s is either an onsite or intersite-centered solution. Setting $v = f + g$ and $w = f - g$ gives

$$L_+ v = -\mathrm{i}\lambda w, \qquad L_- w = \mathrm{i}\lambda v, \tag{17}$$

where

$$L_+ = 2\sum_{m=1}^{\infty} \frac{h^{2m-2}}{(2m)!} \frac{\mathrm{d}^{2m}}{\mathrm{d}\tilde{z}^{2m}} - (3\phi_s^2 - 1), \qquad L_- = 2\sum_{m=1}^{\infty} \frac{h^{2m-2}}{(2m)!} \frac{\mathrm{d}^{2m}}{\mathrm{d}\tilde{z}^{2m}} - (\phi_s^2 - 1). \tag{18}$$

We expand the small eigenvalues bifurcating from the zero eigenvalue for small h as

$$\lambda \sim \varepsilon^{1/2}\lambda_1 + \varepsilon\lambda_2 + \ldots \quad \text{as} \quad \varepsilon \to 0, \tag{19}$$

where ε is exponentially small in h, see the precise definition (36) below. Each λ_j in the expansion (19) is also expanded in powers of h, so this expansion describes an asymptotic trans-series in the small parameter h [4]. We will therefore write

$$\lambda_j \sim \lambda_j^{(0)} + h\lambda_j^{(1)} + \ldots \quad \text{as} \quad h \to 0, \tag{20}$$

for $j = 1, 2, \ldots$. We will later find that the first correction to $\lambda_1^{(0)}$, or $\lambda_1^{(1)}$, is necessary for the asymptotic analysis to match with the numerical calculations. It is possible that $\lambda_j^{(k)}$ can depend on h, but we do require each term in the asymptotic series to be smaller than the preceding terms in the small-h limit.

Similarly to (19), we expand v and w to obtain

$$v \sim v_0 + \varepsilon^{1/2}v_1 + \varepsilon v_2 + \varepsilon^{3/2}v_3 + \ldots, \qquad w \sim w_0 + \varepsilon^{1/2}w_1 + \varepsilon w_2 + \varepsilon^{3/2}w_3 + \ldots, \tag{21}$$

in the limit that h, and hence ε, tends to 0. Due to the translation invariance in the limit, we begin with

$$v_0 = \frac{\mathrm{d}\phi_s}{\mathrm{d}\tilde{z}}, \qquad w_0 = 0, \tag{22}$$

which has the asymptotic behaviour

$$v_0 \sim -\frac{5\Lambda\pi^2}{\sqrt{2}h^5} e^{\sqrt{2}\tilde{z}} e^{-\frac{\sqrt{2}\pi^2}{h}} \cos\left(\frac{2\pi\tilde{z}}{h}\right) \qquad \text{as } \tilde{z} \to \infty,\ h \to 0. \tag{23}$$

This is the growth that needs to be balanced by the $\mathcal{O}(\varepsilon^{1/2})$ term to obtain the leading-order eigenvalue behaviour. Note that the leading-order behaviour in [34] was balanced by an $\mathcal{O}(\varepsilon)$ correction to $L_\pm$. However, in the setting of the discrete problem, we cannot apply a correction to $L_\pm$ in the same way, as the exponential tail is zero on all sites and the correction to $L_\pm$ is therefore zero. Instead, we will enforce the cancellation between v_0 and v_2 directly.

A. Calculating $\lambda_1^{(0)}$

We balance terms from (17), (19), and (21) at $O(\varepsilon^{1/2})$ to obtain

$$L_+ v_1 = 0, \qquad L_- w_1 = \mathrm{i}\lambda_1 \frac{\mathrm{d}\phi_s}{\mathrm{d}\tilde{z}}. \tag{24}$$

The first equation gives $v_1 = a_{11}\Phi_1 + a_{12}\Phi_2$, where Φ_1 and Φ_2 are given by (11)–(12). To prevent exponential growth as $\tilde{z} \to \infty$, we require $a_{12} = 0$. As Φ_1 decays exponentially in the limit $\tilde{z} \to \pm\infty$, we set $a_{11} = 0$ without loss of generality. Balancing the second equation at leading order in h, we find

$$\frac{\mathrm{d}^2 w_1}{\mathrm{d}\tilde{z}^2} - \Big(\phi_0^2 - 1\Big) w_1 = \frac{\mathrm{i}\lambda_1^{(0)}}{\sqrt{2}} \operatorname{sech}^2\left(\frac{\tilde{z}}{\sqrt{2}}\right). \tag{25}$$

The general solution of this inhomogeneous equation is

$$w_1 = \frac{\mathrm{i}\lambda_1^{(0)}}{\sqrt{2}} \left(1 + b_{11} W_1 + b_{12} W_2\right), \tag{26}$$

where W_1 and W_2 are homogeneous solutions given by

$$W_1(\tilde{z}) = \phi_0(\tilde{z}), \qquad W_2(\tilde{z}) = \sqrt{2} - \tilde{z}\,\phi_0(\tilde{z}). \tag{27}$$

In order for this to tend to a constant as $\tilde{z} \to \infty$, which is required to match with the general form given in Theorem 4.10 of [34], we need $b_{12} = 0$. Any other choice of b_{12} will give linear growth as $\tilde{z} \to \infty$, which is not permitted in the dual limit $\varepsilon \to 0$ and $\tilde{z} \to \infty$. Since we have no information about b_{11}, we set

$$w_1 = \frac{\mathrm{i}\lambda_1^{(0)}}{\sqrt{2}} \left(1 + b_{11}\phi_0\right). \tag{28}$$

Balancing terms from (17), (19), and (21) at $O(\varepsilon)$ gives

$$L_+ v_2 = -\mathrm{i}\lambda_1 w_1, \qquad L_- w_2 = \mathrm{i}\lambda_2 v_0. \tag{29}$$

Balancing the first equation from (29) at leading order in h shows that v_2 satisfies

$$\frac{d^2 v_2}{d\tilde{z}^2} - \Big(3\phi_0^2 - 1\Big) v_2 = \frac{\left(\lambda_1^{(0)}\right)^2}{\sqrt{2}} \left(1 + b_{11} \tanh\left(\frac{\tilde{z}}{\sqrt{2}}\right)\right). \tag{30}$$

Solving this gives

$$v_2 = \frac{\lambda_1^{(0)}}{32\sqrt{2}} \operatorname{sech}^2\left(\frac{\tilde{z}}{\sqrt{2}}\right) \left(8\lambda_1^{(0)} \cosh\Big(\sqrt{2}\tilde{z}\Big) + 2\lambda_1^{(0)} \cosh\Big(2\sqrt{2}\tilde{z}\Big) + b_{11}\sqrt{2} \sinh\Big(\sqrt{2}\tilde{z}\Big) - 14\lambda_1^{(0)} - 4b_{11}\tilde{z}\right)$$
$$+ a_{21}\Phi_1 + a_{22}\Phi_2. \tag{31}$$

As before, we set $a_{21} = 0$ without loss of generality. The particular solution grows exponentially in the limits that $\tilde{z} \to \pm\infty$, which is inconsistent with the growth predicted by Theorem 4.10 of [34]. We may choose a_{22} to eliminate exponential growth as $\tilde{z} \to -\infty$ by selecting

$$a_{22} = \frac{\sqrt{2}\left(\lambda_1^{(0)}\right)^2 - b_{11}\lambda_1^{(0)}}{16}. \tag{32}$$

As $\tilde{z} \to \infty$, the asymptotic behaviour of v_2 is a growing exponential,

$$v_2 \sim \frac{\left(\lambda_1^{(0)}\right)^2}{4\sqrt{2}}\, e^{\sqrt{2}\tilde{z}} \quad \text{as} \quad h \to 0,\ \tilde{z} \to \infty. \tag{33}$$

In order to eliminate the growing exponential as $\tilde{z} \to \infty$ from v_0, we require

$$v_0 \sim -\varepsilon v_2 \qquad \text{as} \qquad \tilde{z} \to \infty. \tag{34}$$

Using the asymptotic behaviour of v_0 from (23) and the behaviour of v_2 from (33), this gives

$$\varepsilon \left(\lambda_1^{(0)}\right)^2 \sim -\frac{20\pi^2\Lambda}{h^5} \mathrm{e}^{-\frac{\sqrt{2}\pi^2}{h}} \cos(2\pi(n-n_0)), \tag{35}$$

where we have written the result using the discrete variable n to emphasise the sign difference between onsite-centered (integer n_0) and intersite-centered (half-integer n_0) solutions. We absorb the exponential scaling into ε by setting

$$\varepsilon = \mathrm{e}^{-\frac{\sqrt{2}\pi^2}{h}}. \tag{36}$$

Recalling that $\lambda \sim \varepsilon^{1/2}\lambda_1^{(0)}$ as $h \to 0$, the intersite-centered solutions have

$$\lambda \sim \varepsilon^{1/2}\lambda_1^{(0)} = \pm\frac{\pi\sqrt{20\Lambda}}{h^{5/2}} \mathrm{e}^{-\frac{\sqrt{2}\pi^2}{2h}} \approx \pm\frac{266.004}{h^{5/2}} \mathrm{e}^{-\frac{\sqrt{2}\pi^2}{2h}} \quad \text{as} \quad h \to 0. \tag{37}$$

Since $\lambda_1^{(0)}$ is real, the intersite-centered solutions are unstable. The onsite-centered solutions have

$$\lambda \sim \varepsilon^{1/2}\lambda_1^{(0)} = \pm\frac{\mathrm{i}\pi\sqrt{20\Lambda}}{h^{5/2}} \mathrm{e}^{-\frac{\sqrt{2}\pi^2}{2h}} \approx \pm\frac{266.004\mathrm{i}}{h^{5/2}} \mathrm{e}^{-\frac{\sqrt{2}\pi^2}{2h}} \quad \text{as} \quad h \to 0. \tag{38}$$

B. Calculating $\lambda_1^{(1)}$

As the series terms in the expansion for λ are themselves also series in h, we can calculate the correction to these terms in the small-h limit. This correction is typically significant on the scale at which the numerical calculations will take place. This calculation follows the same steps as in [25], and uses on the expressions for ϕ_0 and ϕ_1 from (5) and (7). In the limit $\tilde{z} \to \tilde{z}_s$, these have the form

$$\phi_0(\tilde{z}) \sim \frac{\sqrt{2}}{\tilde{z}-\tilde{z}_s} + \frac{1}{3\sqrt{2}}(\tilde{z}-\tilde{z}_s) + \ldots, \qquad \phi_1(\tilde{z}) \sim -\frac{\sqrt{2}}{3(\tilde{z}-\tilde{z}_s)^3} + \frac{9+2\mathrm{i}\pi}{24(\tilde{z}-\tilde{z}_s)^2} + \ldots. \tag{39}$$

Combining these expressions yields

$$\phi \sim \frac{\sqrt{2}}{\tilde{z}-\tilde{z}_s} + \frac{1}{3\sqrt{2}}(\tilde{z}-\tilde{z}_s) + h^2\left(-\frac{\sqrt{2}}{3(\tilde{z}-\tilde{z}_s)^3} + \frac{9+2\pi\mathrm{i}}{24(\tilde{z}-\tilde{z}_s)^2}\right) \quad \text{as} \quad h \to 0,\ \tilde{z} \to \tilde{z}_s. \tag{40}$$

Writing this in terms of the inner variable $h\eta = \tilde{z} - \tilde{z}_s$ and letting $\hat{\phi}(\eta) = h\phi(\tilde{z})$ gives a series containing an $\mathcal{O}(h)$ correction term,

$$\hat{\phi}(\eta) \sim \left(\frac{\sqrt{2}}{\eta} - \frac{\sqrt{2}}{3\eta^3}\right) + \frac{(9+2\pi\mathrm{i})h}{24\eta^2} + \mathcal{O}(h^2) \quad \text{as} \quad h \to 0. \tag{41}$$

There is a distinction between this analysis and the work of [20, 25], in that we will not select an alternative inner variable to eliminate the entire $\mathcal{O}(h)$ term, but rather only the imaginary part of the numerator. The remaining contributions are eventually canceled by the complex conjugate term in the exponential asymptotic analysis, and can be ignored in this step. We therefore define the alternative inner variable

$$h\hat{\eta} = \tilde{z} - \tilde{z}_s - \mathrm{i}\frac{\pi h}{12\sqrt{2}},$$

which eliminates the imaginary part of the $\mathcal{O}(h)$ term. This leaves

$$\hat{\phi}(\eta) \sim \left(\frac{\sqrt{2}}{\eta} - \frac{\sqrt{2}}{3\eta^3}\right) + \frac{9h}{24\eta^2} + \mathcal{O}(h^2) \quad \text{as} \quad h \to 0. \tag{42}$$

This captures the first correction to the imaginary part of the true pole location, which is important for the eigenvalue calculation. Using an identical argument to [25], the adjusted exponentially small contribution based on (13) becomes

$$\phi_{\rm exp}(\tilde{z}) \sim -\frac{2\pi {\rm i}\Phi(\tilde{z})}{h^\gamma}\, {\rm e}^{-\frac{\sqrt{2}\pi^2}{h}} {\rm e}^{-\frac{\pi^2 h}{24}} + {\rm c.\ c.} \quad \text{as} \quad h \to 0. \tag{43}$$

In the dual limit $\tilde{z} \to \infty$ and $h \to 0$, this term has the behaviour

$$\phi_{\rm exp}(\tilde{z}) \sim -\frac{2\pi}{h^4}\left(\frac{5\Lambda}{4\sqrt{2}}{\rm e}^{\sqrt{2}\tilde{z}}\right) e^{-\frac{\sqrt{2}\pi^2}{h}} \left(1 - \frac{\pi^2 h}{12\sqrt{2}}\right) \sin\left(\frac{2\pi\tilde{z}}{h}\right) \quad \text{as} \quad h \to 0,\ \tilde{z} \to \infty, \tag{44}$$

and hence we find that

$$\lambda_1^{(1)} = -\frac{\pi^2 \lambda_1^{(0)}}{12\sqrt{2}}. \tag{45}$$

Thus, the corrected eigenvalue at the order of $\varepsilon^{1/2}$ is given by

$$\lambda \sim \varepsilon^{1/2}\lambda_1^{(0)}\left(1 - \frac{\pi^2 h}{12\sqrt{2}}\right) \approx \pm(266.004 - 154.700h)h^{-5/2}{\rm e}^{-\frac{\sqrt{2}\pi^2}{2h}} \quad \text{as} \quad h \to 0 \tag{46}$$

for intersite-centered solutions, and

$$\lambda \sim \varepsilon^{1/2}\lambda_1^{(0)}\left(1 - \frac{\pi^2 h}{12\sqrt{2}}\right) \approx \pm{\rm i}(266.004 - 154.700h)h^{-5/2}{\rm e}^{-\frac{\sqrt{2}\pi^2}{2h}} \quad \text{as} \quad h \to 0 \tag{47}$$

for onsite-centered solutions.

As in [25], this predicts that the onsite-centered eigenvalues are imaginary at leading order in ϵ. However, in order to show that these solutions are also unstable, we need to find the correction term λ_2, which is turned out to be real. This will connect with the expectation based on numerical observations [14, 23] about the instability of these onsite solutions due to a complex eigenvalue quartet.

C. Calculating $\lambda_2^{(0)}$

Balancing the second equation from (29) at leading order in h gives the equation for w_2,

$$w_2 = {\rm i}\left(\frac{\lambda_2^{(0)}}{\sqrt{2}} + b_{21}W_1 + b_{22}W_2\right), \tag{48}$$

where W_1 and W_2 are given by (27). The coefficient b_{21} does not affect the present calculation. From the analysis in Theorem 4.10 of [34], we know that the perturbation w_2 can grow with the rate of $\mathcal{O}(\tilde{z}\varepsilon)$ as $\tilde{z} \to \infty$ and $\varepsilon \to 0$. To specify b_{22}, we must match the expansion for w against the corresponding large-$\tilde{z}$ result from [34].

1. *Determining the constant b_{22}*

From (4.12) in [34], we know the limiting behaviour of w as $\tilde{z} \to \pm\infty$. Expressed in the present variables (noting that c from [34] is equal to 1 here, and that w is scaled by i in our formulation), it is

$$w \to -2{\rm i}a_+ + 2{\rm i}a_+\tilde{z}\left(\lambda_1\varepsilon^{1/2} + \lambda_2\varepsilon + \ldots\right) \quad \text{as} \quad \tilde{z} \to \infty,\ \varepsilon \to 0, \tag{49}$$

$$w \to -2{\rm i}a_- - 2{\rm i}a_-\tilde{z}\left(\lambda_1\varepsilon^{1/2} + \lambda_2\varepsilon + \ldots\right) \quad \text{as} \quad \tilde{z} \to -\infty,\ \varepsilon \to 0. \tag{50}$$

where $a_\pm$ are constants in $\tilde{z}$ that can scale with ε. We found

$$w \sim \frac{{\rm i}\varepsilon^{1/2}\lambda_1}{\sqrt{2}}(1 + b_{11}\phi_0) + {\rm i}\varepsilon\left(\frac{\lambda_2^{(0)}}{\sqrt{2}} + b_{21}\phi_0 + b_{22}(\sqrt{2} - \tilde{z}\phi_0)\right) + \ldots \quad \text{as} \quad \varepsilon \to 0, \tag{51}$$

where $\lambda_1 \sim \lambda_1^{(0)} + h\lambda_1^{(1)} + \ldots$. We require the asymptotic behaviour as $\tilde{z} \to \pm\infty$ to balance against (49), which is

$$w \sim \mathrm{i}\varepsilon^{1/2}\left(\frac{\lambda_1}{\sqrt{2}} + b_{11}\right) + \mathrm{i}\varepsilon\left(\frac{\lambda_2}{\sqrt{2}} + b_{21} + \sqrt{2}b_{22} - b_{22}\tilde{z}\right) + \ldots \quad \text{as} \quad \tilde{z} \to \infty,\ \varepsilon \to 0, \tag{52}$$

$$w \sim \mathrm{i}\varepsilon^{1/2}\left(\frac{\lambda_1}{\sqrt{2}} - b_{11}\right) + \mathrm{i}\varepsilon\left(\frac{\lambda_2}{\sqrt{2}} + b_{21} + \sqrt{2}b_{22} + b_{22}\tilde{z}\right) + \ldots \quad \text{as} \quad \tilde{z} \to \infty,\ \varepsilon \to 0. \tag{53}$$

Balancing the leading-order terms in (49)–(50) and (52)–(53) as $\varepsilon \to 0$ gives

$$a_+ = -\frac{\sqrt{2}\lambda_1 + 2b_{11}}{4}, \qquad a_- = -\frac{\sqrt{2}\lambda_1 - 2b_{11}}{4}. \tag{54}$$

Now we balance the $\mathcal{O}(\tilde{z}\varepsilon)$ terms of (49)–(50) and (52)–(53) in the dual limit to find

$$b_{11} = 0, \qquad b_{22} = \frac{\lambda_1^2}{2\sqrt{2}} \sim \frac{\left(\lambda_1^{(0)}\right)^2}{2\sqrt{2}} \quad \text{as} \quad h \to 0. \tag{55}$$

Using (55) in (32) gives

$$a_{22} = \frac{\lambda_1^2}{8\sqrt{2}} \sim \frac{\left(\lambda_1^{(0)}\right)^2}{8\sqrt{2}} \quad \text{as} \quad h \to 0. \tag{56}$$

We have now determined all of the constants we require to complete the analysis.

2. Fredholm alternative

Balancing terms of (17), (19), and (21) at $\mathcal{O}(\varepsilon^{3/2})$ gives

$$L_+ v_3 = -\mathrm{i}\lambda_1 w_2 - \mathrm{i}\lambda_2 w_1. \tag{57}$$

To ensure that the solution does not experience exponential growth in the limit that $\tilde{z} \to \infty$, this system must satisfy the Fredholm alternative. In this case, that implies

$$-\mathrm{i}\lambda_1\langle V_1, w_2\rangle - \mathrm{i}\lambda_2\langle V_1, w_1\rangle = 0. \tag{58}$$

Evaluating this explicitly with w_1 in (28) and w_2 in (48) gives

$$\frac{\lambda_1\lambda_2}{2} + \frac{\lambda_1}{8}(\sqrt{2}\lambda_1^2 + 4\lambda_2) = 0, \quad \Rightarrow \quad \lambda_2 = -\frac{\lambda_1^2}{4\sqrt{2}}. \tag{59}$$

Since λ_1 is imaginary, this quantity is real and the solution is unstable. Furthermore, we have been able to calculate the correction to the eigenvalue explicitly. For the onsite-centered solution, this gives the prediction for λ_2

$$\lambda_2 = -\frac{\lambda_1^2}{4\sqrt{2}} \sim \frac{5\pi\Lambda}{\sqrt{2}h^5}\left(1 - \frac{\pi^2 h}{12\sqrt{2}}\right)^2 \sim \frac{5\pi^2\Lambda}{\sqrt{2}h^5}\left(1 - \frac{\pi^2 h}{6\sqrt{2}}\right) = \lambda_2^{(0)} + h\lambda_2^{(1)} \quad \text{as} \quad h \to 0, \tag{60}$$

From symmetry arguments, this in fact predicts four eigenvalues in total, described by

$$\lambda \sim \pm\varepsilon^{1/2}\lambda_1 \pm \varepsilon\lambda_2 \quad \text{as} \quad h \to 0, \tag{61}$$

where the two sign choices are made independently, $\lambda_1^{(0)}$ and $\lambda_1^{(1)}$ are imaginary, $\lambda_2^{(0)}$ and $\lambda_2^{(1)}$ are real, and ε is a real scaling factor that is exponentially small in the limit $h \to 0$. Hence, we find that the real part of the eigenvalues is

$$\epsilon\lambda_2 \sim \pm\frac{5\pi^2\Lambda}{\sqrt{2}h^5}\left(1 - \frac{\pi^2 h}{6\sqrt{2}}\right)\mathrm{e}^{-\frac{\sqrt{2}\pi^2}{h}} \approx \pm(12508.376 - 14549.043h)h^{-5}\mathrm{e}^{-\frac{\sqrt{2}\pi^2}{h}} \quad \text{as} \quad h \to 0. \tag{62}$$

This means that even though the leading-order solution for λ_1 is imaginary for the onsite-centered solution, the real correction term for λ_2 ensures that the onsite-centered solution is unstable.

D. Comparison of λ_2 with the pinning theory from [34]

We show that the prediction of the correction λ_2 in (59) can be re-derived from the theory of the soliton pinning in an external potential in [34]. Moreover, this allows us to compute the effective Peierls–Nabarro potential due to the discrete lattice.

We recall from [34] that the continuum NLS equation with an external potential was considered in the form:

$$iu_t = -\frac{1}{2}u_{xx} + f(|u|^2)\,u + \epsilon V(x)\,u. \tag{63}$$

It was shown in Theorems 2.12 and 4.11 of [34] that the dark soliton with the profile ϕ_0 satisfying $|\phi_0(x)| \to 1$ as $|x| \to \infty$ are pinned as $\epsilon \to 0$ to simple zeros s_0 of the effective potential $M'(s)$ given by

$$M'(s) = \int_{\mathbb{R}} V'(x)\left[1 - \phi_0^2(x-s)\right] dx, \tag{64}$$

while $M''(s_0)$ determines eigenvalues λ of the spectral stability problem according to the characteristic equation

$$\text{Re}\,\lambda > 0: \qquad \left(P'\big|_{v\downarrow 0}\right)\lambda^2 - \epsilon\,\frac{\left(S'\big|_{v\downarrow 0}\right)^2 M''(s_0)}{2\sqrt{f'(1)}\left(P'\big|_{v\downarrow 0}\right)}\,\lambda + \epsilon\,M''(s_0) = \mathcal{O}(\epsilon^2), \tag{65}$$

where $P[u]$ and $S[u]$ were the conserved (renormalized) momentum and the conserved phase difference defined as

$$P[u] = \frac{i}{2}\int_{\mathbb{R}} (\bar{u}u_x - u\bar{u}_x)\left(1 - \frac{1}{|u|^2}\right) dx \tag{66}$$

and

$$S[u] = \frac{i}{2}\int_{\mathbb{R}} \left(\frac{\bar{u}_x}{\bar{u}} - \frac{u_x}{u}\right) dx. \tag{67}$$

These conserved quantities were computed on the family of traveling dark soliton $u = \phi(x - vt)$ parametrized by the wave speed v and the prime stands for the derivative with respect to v as $v \downarrow 0$. In the most interesting case of $f(s) = s$, the exact traveling dark solitons (up to the e^{-it} phase factor) exists in the form:

$$\phi(x - vt) = k\tanh(k(x - vt)) + iv, \qquad k = \sqrt{1 - v^2}, \tag{68}$$

To implement these results to the case of our studies, we notice the $1/2$ factor mismatch in front of the Laplacian term. Hence for our setting, we need to rescale x and v by $\frac{1}{\sqrt{2}}$ and replace the solutions of Eq. (68) to the form:

$$\phi(x - vt) = k\tanh\left(\frac{k}{\sqrt{2}}(x - vt)\right) + i\frac{v}{\sqrt{2}}, \qquad k = \sqrt{1 - \frac{v^2}{2}}. \tag{69}$$

On the other hand, the characteristic equation (65) and the conserved quantities (66) and (67) remain in the same form. Using the exact solution (69), we obtain

$$P'\big|_{v\downarrow 0} = 2\sqrt{2}, \qquad S'\big|_{v\downarrow 0} = \sqrt{2}, \tag{70}$$

so that the characteristic equation (65) can be written in the form:

$$\text{Re}\,\lambda > 0: \qquad \lambda^2 + \frac{\epsilon}{2\sqrt{2}}M''(s_0)\left(1 - \frac{\lambda}{2\sqrt{2}}\right) = \mathcal{O}(\epsilon^2). \tag{71}$$

Expanding like in (19),

$$\lambda = \epsilon^{1/2}\lambda_1 + \epsilon\lambda_2 + \mathcal{O}(\epsilon^{3/2}),$$

we obtain from (71) that

$$\lambda_1^2 + \frac{1}{2\sqrt{2}} M''(s_0) = 0, \quad \lambda_2 = \frac{1}{16} M''(s_0) = -\frac{\lambda_1^2}{4\sqrt{2}}, \tag{72}$$

where the second relation coincides with (59). By using (35) and the first relation, we recover the derivative of the effective potential as

$$M''(s_0) \sim \frac{40\sqrt{2}\pi^2\Lambda}{h^5} \mathrm{e}^{-\frac{\sqrt{2}\pi^2}{h}} \cos(2\pi s_0). \tag{73}$$

Integration recovers the effective Peierls–Nabarro potential

$$M'(s) \sim \frac{20\sqrt{2}\pi\Lambda}{h^5} \mathrm{e}^{-\frac{sqrt2\pi^2}{h}} \sin(2\pi s),$$

which replaces the effective continuous potential (64) in the discrete setting.

IV. NUMERICAL RESULTS

Before presenting our numerical results, we briefly summarize the currently available predictions regarding the eigenvalues associated with the intersite and onsite solitary waves.

We start with the simpler intersite case which was considered theoretically near the anti-continuum limit in [35] and near the continuum one of in [2]. In this case, the discrete solitary wave is well-known (already from the seminal work of [14]) to possess a real eigenvalue pair in the corresponding linearization. This pair is known to bifurcate from the origin of the spectral plane along the real axis *already in the vicinity of the anti-continuum limit* (i.e., for lattice spacing $h \to \infty$) [35]. The associated pair *remains real for all* h and finally approaches the origin to "restore" translational invariance through an exponentially small dependence as $h \to 0$ [2]. Revisiting relevant quantitative details, we recall that the work of [2] found the relevant eigenvalue to be

$$\lambda \approx \pm\sqrt{4\sqrt{2}\pi^2 2534.73} h^{-5/2} e^{-\frac{\sqrt{2}\pi^2}{2h}}, \tag{74}$$

where, to enable direct comparison, we have continued the calculation of the constant from [2] to have the equivalent precision to our calculation of the unstable eigenvalue λ. The numerical computations of [23] deemed this prediction to bear the correct functional dependence on h, yet miss the leading order prefactor. The best fit numerical approximation, motivated by the corresponding expression for bright discrete solitary waves in [25], was found to be:

$$\lambda \approx \pm\left(265.238 - 135.983h\right) h^{-5/2} e^{-\frac{\sqrt{2}\pi^2}{2h}} \tag{75}$$

Our predictions of the unstable eigenvalue λ for the intersite solution, based on [34], are found from (71) and (73),

$$\lambda \approx \pm\sqrt{2\sqrt{2}\pi^2 2534.73 h^{-5} e^{-\frac{\sqrt{2}\pi^2}{h}}} = 266.004 h^{-5/2} e^{-\frac{\sqrt{2}\pi^2}{2h}} \tag{76}$$

which is in *excellent agreement* with the leading order of the multiprecision numerical findings of [23]. The reason for the discrepancy in (74) from [2], compared to the correct prediction (76), is due to the error in solving the linear inhomogeneous equation (25) for the correction term w_1. The solution was chosen to be unbounded in [2], whereas the relevant solution must be bounded as in our Eq. (28) due to $b_{12} = 0$. The correct prediction (76) is obtained from the bounded soluton for w_1 independently on the value of b_{11}.

In the case of onsite solution, the binomial of (71), (72), and (73) yields (again up to exponentially small corrections):

$$\lambda \approx \pm i 266.004 h^{-5/2} e^{-\frac{\sqrt{2}\pi^2}{2h}} \pm 12508.376 h^{-5} e^{-\frac{\sqrt{2}\pi^2}{h}} \tag{77}$$

The work of [23] provides a fit only in a neighborhood far from $h \to 0$, hence we do not compare (77) to [23].

Our *full* exponential asymptotics prediction for the case of intersite soluton, incorporating the next order correction to the leading order, is given by (46) and thus improving upon Eq. (76) reads:

$$\Lambda \approx \pm(266.004 - 154.7h)h^{-5/2}e^{-\frac{\sqrt{2}\pi^2}{2h}} \tag{78}$$

which can be seen to be highly proximal —in its leading order prediction— to the multiprecision numerical fit of [23]. It is also worthwhile to note how our next order correction improves upon the relevant prediction in comparison to the numerical fit, as the latter was performed with data at some distance from the $h \to 0$ limit.

The summary of all the analytical and numerical results of earlier studies [2, 23, 34] culminating into this work are summarized in Table I. The table illustrates at a glance how the present work's analysis amends the prediction of [2], extends the leading order adaptation (to the present discrete setting) of [34], while matching very closely the best fit numerical findings of [23].

Table I: Comparison of Different Predictions for the IS Discrete Soliton Positive Real Eigenvalue

Numerical Prefactor	Reference Source	Origin
$\sqrt{4\sqrt{2}\pi^2 2534.73}$	[2]	Analytical
$265.238 - 135.983\,h$	[23]	Numerical Fit
$\sqrt{2\sqrt{2}\,\pi^2\,2534.73} \equiv 266.004$	[34]	Analytical
$266.004 - 154.7\,h$	Present Work	Analytical

The numerical prediction of Eq. (78) is given by the red dashed line in both panels of Fig. 2. The leading order result (76) is captured by the black dash-dotted line. The latter can be seen (through a suitable magnification) to start deviating from the numerical results for $h \approx 0.2$. Remarkably, the prediction of Eq. (78) cannot be really distinguished from the numerics over the scale of the graph, i.e., even up to $h \approx 0.7$ and quite remarkably for about 35 orders of magnitude of the variation of the relevant real eigenvalue (see the right panel). The left panel multiplies the eigenvalue by both the power and the exponential, lucidly illustrating the approach to the asymptotic prediction as $h \to 0$. These results were obtained with computations using the Multiprecision Computing Toolbox within Matlab (but with smaller lattices involving 1000 nodes; cf. with the larger lattice computations below).

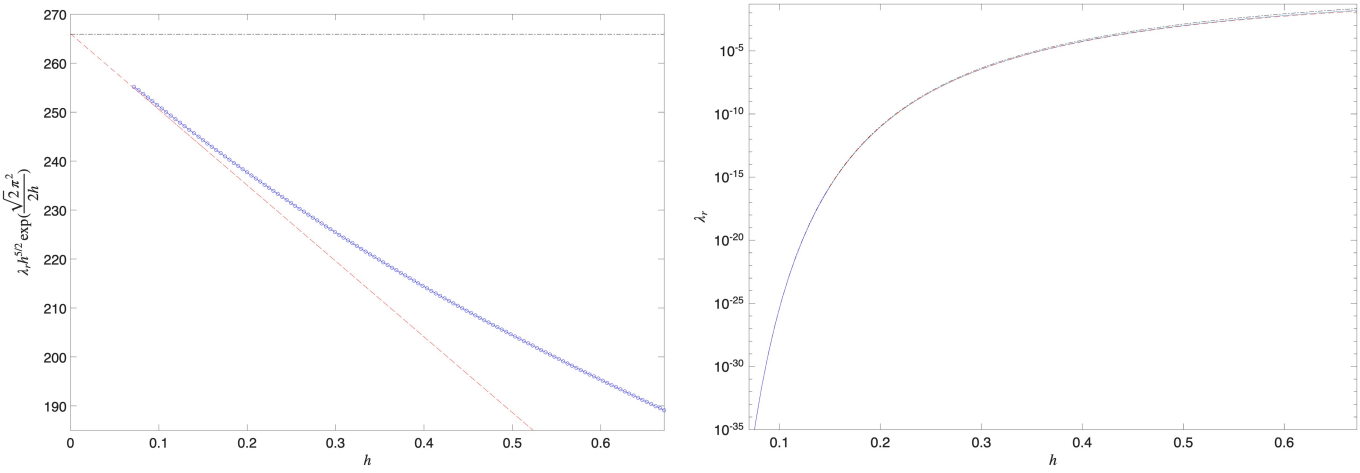

Figure 2: The eigenvalue of the intersite solution is shown both upon its multiplication by $h^{5/2}e^{\frac{\sqrt{2}\pi^2}{2h}}$ (which renders its asymptotic form transparent) in the left panel and "as is" in the right panel. The numerical data are shown in blue, while the red dashed provides the exponential asymptotic prediction of Eq. (78) and the dash-dotted black curve yields the leading order approximation of Eq. (76).

Figure 3 presents similar results to the ones above but for the onsite solution. Here, a clarification needs to be made

(which is partially aligned with the explanations of [23]). In order to use the Multiprecision Computing Toolbox, we found it necessary to restrict our considerations to computations with 1000 nodes. In that case, the continuous spectrum becomes discretized. Accordingly, as $h \to 0$, the complex quartet associated with the onsite mode instability traces gaps between the discretized eigenvalues and accordingly returns to the imaginary axis. Similar findings have been reported in [14] (see Fig. 2 therein and the corresponding "arcs" of eigenvalues jumping in and out of the imaginary axis), as well as in [34] (see, e.g., Fig. 4 of that work, and the associated non-monotonic dips therein). As the continuum limit is approached the final "crossing" of this sort takes place around $h \approx 0.8$, hence the "scatter" of eigenvalues near that neighborhood, as observed in the left panel of Fig. 3. For lower values of h and as the continuum limit is approached, the numerical problem, due to its finite size, has the translational eigenvalue approaching the origin as purely imaginary. Nevertheless, and remarkably so, this imaginary approach is found to be excellently aligned with the theoretical prediction for the imaginary part of the eigenvalue as given in Eq. (77) to leading order. In fact, with the next-order correction to the leading order given by (47) and (62), we have

$$\lambda \approx \pm i(266.004 - 154.700h)h^{-5/2}e^{-\frac{\sqrt{2}\pi^2}{2h}} \pm (12508.376 - 14549.043h)h^{-5}e^{-\frac{\sqrt{2}\pi^2}{h}}. \tag{79}$$

The Multiprecision Computing Toolbox enables capturing this prediction very accurately to several orders of magnitude as can be seen in the right panel of Figure 3. On the other hand, the leading order prediction can again be visibly discerned to start gradually deviating around $h \approx 0.2$. Nevertheless, the dominant prediction can be deemed to be extremely accurate up to $h \approx 0.2$ and the next order correction, similarly, even beyond $h \approx 0.5$.

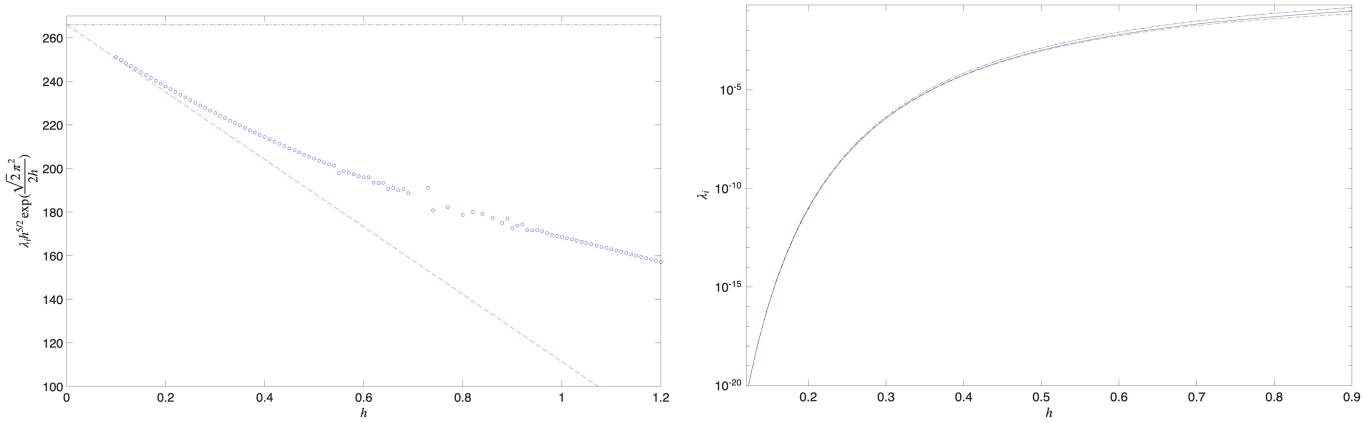

Figure 3: Similar results to Figure 2 but for the imaginary part of the complex eigenvalue associated with the onsite solution. The prediction is essentially the same as above (now on the imaginary axis) and the agreement of both the leading order asymptotics (77) and of the next-order correction (79) documented again by the black, dash-dotted and the red dashed curves, respectively.

The above considerations clearly underscore the difficulty of capturing the real part of the eigenvalue quartet all the way to $h \to 0$, a difficulty that forced the authors of [23] to perform a fit only up to $h \approx 0.9$. The real part of the corresponding quartet as computed in much larger lattices of 3000 nodes (but without the Multiprecision Computing Toolbox, as the latter computation proved to be infeasible with our computational resources) is shown Fig. 4 down to $h \approx 0.9$. The leading-order prediction of Eq. (77) is compared to the corresponding numerical result in the figure, with the deviation being comparable to what one can observe in the right panel of Fig. 3 for the same parameter range. While we have every expectation that the leading-order prediction provided matches very well the numerical, infinite lattice result as $h \to 0$, our computational capabilities do not allow a full confirmation of that fact at present.

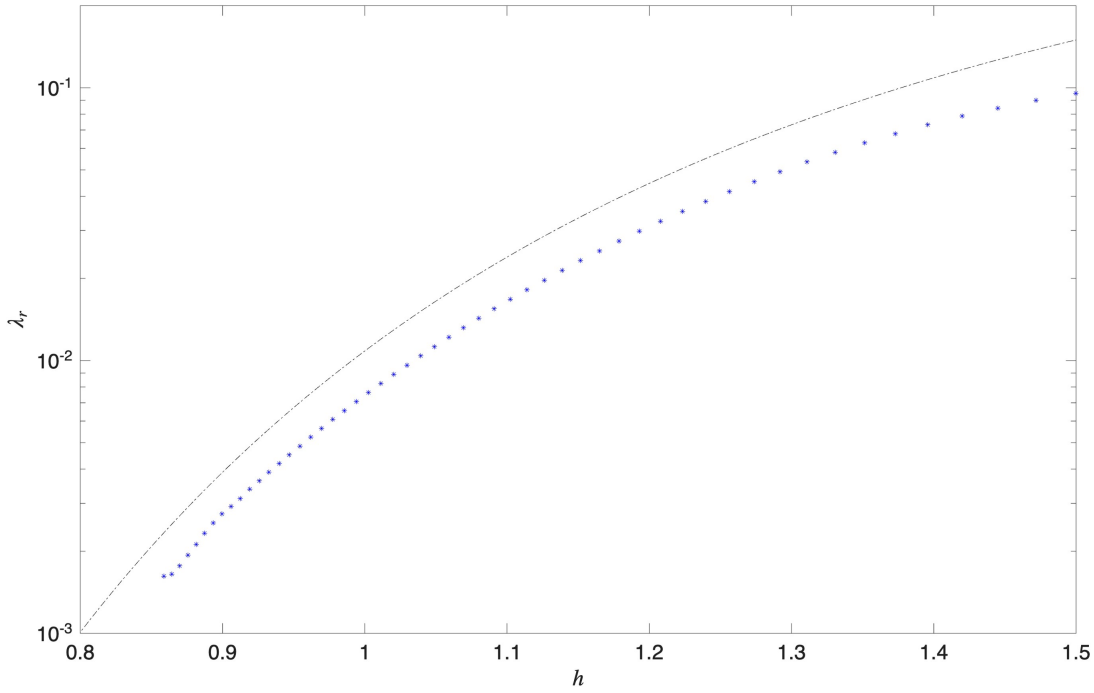

Figure 4: Numerical results for the real (unstable) part of the complex eigenvalue of the onsite configuration. The leading-order asymptotics of Eq. (77) is given by the black dash-dotted curve.

V. CONCLUSIONS AND FUTURE CHALLENGES

In the present work we have revisited a problem with considerable history, as well as with very broad applicability. This concerns the implications of discreteness and its associated breaking of translational invariance in connection with the spectral features of the multiple (intersite and onsite) dark discrete solitary waves that emerge through the discretization of the model as potential stationary states. In line with earlier studies, the breaking of translational invariance leads to beyond-all-algebraic order (indeed exponentially small) eigenvalues, modulated by a power of $h^{-\alpha}$, where h is the lattice spacing. While early studies such as [12] and [15] captured the numerical features of the bright solitary wave spectral analysis, it was not until recently that the focusing problem was fully analyzed in terms of the leading order [2, 25] and even its next order correction [25] for the eigenvalue associated with translation. Nevertheless, the technical complexity of the dark solitary waves of the defocusing DNLS, already outlined in the seminal work of [14], have meant that the latter case has remained elusive for a quarter of a century with recent efforts [2, 23] improving on the relevant numerics, yet not providing a conclusive theoretical answer. The present work has been able to achieve that *both* for the intersite dark solitary waves (and their real eigenvalue pair) and for the considerably more elaborate onsite dark solitary waves (bearing a complex eigenvalue quartet near the continuum limit). In the process, we have also established a firm connection with the analysis of pinning of the dark solitary waves in [34] in the presence of external potentials. This connection may bear further fruit towards describing the motion of the discrete solitary waves, by analogy to the corresponding equations of motion obtained in [34].

In addition to this dynamical vein for defocusing DNLS dark solitons, we believe that this line of asymptotic efforts may lead to numerous further developments. For instance, a topic that has received considerable attention not only in the context of the DNLS [12], but also in other settings such as the discrete sine-Gordon [15, 21] has been the study of internal modes that bifurcate from the continuous spectrum, leading associated resonances —sitting at the edge of the spectral band— to transform into point spectrum eigenvalues. Although such modes were originally deemed to be power law in their bifurcations [19, 21], it was subsequently discovered that they bear both exponential and power

law characteristics [15, 16]. Nevertheless, associated eigenvalue dependences on the lattice spacing never reached the level of accuracy of recent predictions based on exponential asymptotics, leaving an important open problem.

An additional equally intriguing vein concerns exploring models of either generalized power or of generalized dimension in the context of the DNLS [13, 27], as these models possess stability variations (even for onsite branches) and invervals of bistability. It would be interesting to explore how these models approach the continuum limit as a function of the dimension d or the exponent p of the nonlinearity and to explore how exponential asymptotics may be able to capture the dependence not only on the lattice spacing but also on such as an additional parameter such as p.

Finally, recent work has explored the setting of the so-called "Maxwell fronts", i.e., kinks that arise from the competition of two different nonlinearities, such as, e.g., quadratic and cubic, or cubic and quintic. These kinks have been demonstrated to possess intriguing stability properties not only in one dimension [11], but also in higher dimensions where they are transversely stable [29]. The work of [3] has explored such kinks in the realm of the lattice where they were shown to be continued from the anti-continuum all the way to the continuum limit. A further characterization of their stability properties based on the methods proposed herein is a particularly interesting subject for future work.

Acknowledgements. CJL acknowledges support from Australian Research Council Discovery Project DP240101666. This research was supported by the U.S. National Science Foundation under the award PHY-2408988 (PGK). This research was partly conducted while P.G.K. was visiting the Okinawa Institute of Science and Technology (OIST) through the Theoretical Sciences Visiting Program (TSVP), the University of Sydney through the visitor program of the Sydney Mathematical Research Institute (SMRI) and the Department of Mechanical Engineering at Seoul National University through a Fulbright Fellowship. Their support is gratefully acknowledged. Finally, this work was also supported by a grant from the Simons Foundation [SFI-MPS-SFM-00011048, P.G.K].

[1] M. J. Ablowitz, B. Prinari, and A. D. Trubatch. *Discrete and Continuous Nonlinear Schrödinger Systems*. Cambridge University Press, Cambridge, 2004.

[2] F. T. Adriano, A. N. Hasmi, R. Kusdiantara, and H. Susanto. Exponential asymptotics of dark and bright solitons in the discrete nonlinear schrödinger equation. *Physica D*, 481:134848, 2025.

[3] F. T. Adriano and H. Susanto. Maxwell fronts in the discrete nonlinear Schrödinger equations with competing nonlinearities. *Stud. Appl. Math.*, 156(2):e70191, 2026.

[4] I. Aniceto, G. Başar, and R. Schiappa. A primer on resurgent transseries and their asymptotics. *Phys. Rep.*, 809:1–135, 2019.

[5] S. J. Chapman and D. B. Mortimer. Exponential asymptotics and Stokes lines in a partial differential equation. *Proc. Roy. Soc. Lond. A*, 461(2060):2385–2421, 2005.

[6] T. Cretegny and S. Aubry. Spatially inhomogeneous time-periodic propagating waves in anharmonic systems. *Phys. Rev. B*, 55:R11929–R11932, May 1997.

[7] J. C. Eilbeck and M. Johansson. The discrete nonlinear Schrödinger equation - 20 years on. *Localization and Energy Transfer in Nonlinear Systems*, pages pp. 44–67, 2003.

[8] S. Flach and A. V. Gorbach. Discrete breathers — Advances in theory and applications. *Phys. Rep.*, 467(1-3):1–116, 2008.

[9] S. Flach and K. Kladko. Moving discrete breathers? *Physica D*, 127(1):61 – 72, 1999.

[10] J. Gómez-Gardeñes, F. Falo, and L. M. Floría. Mobile localization in nonlinear Schrödinger lattices. *Phys. Lett. A*, 332(3):213–219, 2004.

[11] J. Holmer, P. G. Kevrekidis, and D. E. Pelinovsky. Orbital stability of kinks in the nls equation with competing nonlinearities, 2025.

[12] M. Johansson and S. Aubry. Growth and decay of discrete nonlinear Schrödinger breathers interacting with internal modes or standing-wave phonons. *Phys. Rev. E*, 61:5864–5879, May 2000.

[13] M. Johansson, S. Aubry, Y. B. Gaididei, P. L. Christiansen, and K. Ø. Rasmussen. Dynamics of breathers in discrete nonlinear Schrödinger models. *Physica D*, 119(1):115–124, 1998.

[14] M. Johansson and Y. S. Kivshar. Discreteness-induced oscillatory instabilities of dark solitons. *Phys. Rev. Lett.*, 82:85–88, Jan 1999.

[15] T. Kapitula and P. G. Kevrekidis. Stability of waves in discrete systems. *Nonlinearity*, 14(3):533, may 2001.

[16] T. Kapitula, P. G. Kevrekidis, and C. K. R. T. Jones. Soliton internal mode bifurcations: Pure power law? *Phys. Rev. E*, 63:036602, Feb 2001.

[17] P. G. Kevrekidis. *The Discrete Nonlinear Schrödinger Equation*. Springer-Verlag, Heidelberg, 1st edition, 2009.

[18] P. G. Kevrekidis, G. J. Herring, S. Lafortune, and Q. E. Hoq. The higher-dimensional Ablowitz–Ladik model: From (non-)integrability and solitary waves to surprising collapse properties and more exotic solutions. *Phys. Lett. A*, 376(8):982–986, 2012.

[19] P. G. Kevrekidis and C. K. R. T. Jones. Bifurcation of internal solitary wave modes from the essential spectrum. *Phys. Rev. E*, 61:3114–3121, Mar 2000.

[20] J. R. King and S. J. Chapman. Asymptotics beyond all orders and Stokes lines in nonlinear differential-difference equations. *Eur. J. Appl. Math.*, 12(4):433–463, 2001.

[21] Y. S. Kivshar, D. E. Pelinovsky, T. Cretegny, and M. Peyrard. Internal modes of solitary waves. *Phys. Rev. Lett.*, 80:5032–5035, Jun 1998.

[22] Yuri S. Kivshar and David K. Campbell. Peierls-Nabarro potential barrier for highly localized nonlinear modes. *Phys. Rev. E*, 48:3077–3081, Oct 1993.

[23] R. Kusdiantara, F. T. Adriano, and H. Susanto. Multiprecision computation of bright and dark solitons in the discrete nonlinear Schrödinger equation. Preprint, 2025.

[24] C. J. Lustri, I. Aniceto, and P. G. Kevrekidis. Borel-Padé exponential asymptotics for the discrete nonlinear Schrödinger model with next-to-nearest neighbour interactions. *SIAM J. Appl. Math.*, 2026 (In press).

[25] C. J. Lustri, P. G. Kevrekidis, and S. Jonathan Chapman. Exponential asymptotics for translational modes in the discrete nonlinear Schrödinger model. *Quart. Appl. Math.*, 2025. Published electronically June 5, 2025.

[26] R S MacKay and S Aubry. Proof of existence of breathers for time-reversible or Hamiltonian networks of weakly coupled oscillators. *Nonlinearity*, 7(6):1623, nov 1994.

[27] B. Malomed and M. I. Weinstein. Soliton dynamics in the discrete nonlinear Schrödinger equation. *Phys. Lett. A*, 220(1):91–96, 1996.

[28] B. A. Malomed and P. G. Kevrekidis. Discrete vortex solitons. *Phys. Rev. E*, 64:026601, Jul 2001.

[29] S. I. Mistakidis, G. Bougas, G. C. Katsimiga, and P. G. Kevrekidis. Generic transverse stability of kink structures in atomic and optical nonlinear media with competing attractive and repulsive interactions. *Phys. Rev. Lett.*, 134:123402, Mar 2025.

[30] A. B. Olde Daalhuis, S. J. Chapman, J. R. King, J. R. Ockendon, and R. H. Tew. Stokes phenomenon and matched asymptotic expansions. *SIAM J. Appl. Math.*, 55(6):1469–1483, 1995.

[31] O. F. Oxtoby and I. V. Barashenkov. Moving solitons in the discrete nonlinear Schrödinger equation. *Phys. Rev. E*, 76:036603, Sep 2007.

[32] D. E. Pelinovsky. Translationally invariant nonlinear Schrödinger lattices. *Nonlinearity*, 19(11):2695, oct 2006.

[33] D. E. Pelinovsky. *Localization in Periodic Potentials: From Schrödinger Operators to the Gross–Pitaevskii Equation*. London Mathematical Society Lecture Note Series. Cambridge University Press, 2011.

[34] D. E. Pelinovsky and P. G. Kevrekidis. Dark solitons in external potentials. *Z. Angew. Math. Phys.*, 59:559–599, 2008.

[35] D. E. Pelinovsky and P. G. Kevrekidis. Stability of discrete dark solitons in nonlinear Schrödinger lattices. *J. Phys. A*, 41(18):185206, apr 2008.

[36] M. Peyrard and M. D. Kruskal. Kink dynamics in the highly discrete sine-Gordon system. *Physica D*, 14(1):88–102, 1984.